ISSN 0024-4902, Lithology and Mineral Resources, 2020, Vol. 55, No. 5, pp. 327–337. © Pleiades Publishing, Inc., 2020.
Russian Text © The Author(s), 2020, published in Litologiya i Poleznye Iskopaemye, 2020, No. 5, pp. 387–399.

Facies Structure and Quantitative Parameters of Pleistocene Sedimentation on the Deep-Sea Floor of the Southern Pacific Ocean and in the Scotia Sea

M. A. Levitan[a], *, T. N. Gelvi[a], and L. G. Domaratskaya[a]

[a]*Vernadsky Institute of Geochemistry and Analytical Chemistry RAS, Moscow, 119991 Russia*

**e-mail: m-levitan@mail.ru*

Received January 15, 2020; revised January 28, 2020; accepted February 26, 2020

Abstract—Based on the data from long sediment cores retrieved by R/V *Eltanin* (United States) during the 1950s–1960s, Neo- and Eopleistocene lithofacies maps of the southern Pacific Ocean (scale 1 : 20000000) and Scotia Sea (scale 1 : 10000000) were compiled for the first time. For the Scotia Sea, schemes of isopachites are shown on the respective lithofacies maps. All maps are processed with the volumetric method proposed by A.B. Ronov. The results revealed that accumulation rates of the terrigenous and siliceous sediments increased during the Pleistocene in both sedimentation basins due to neotectonic activity in the Antarctic Peninsula, which enhanced fluxes of not only terrigenous matter but also nutrients delivered by melted waters to the photosynthesis zone via vertical circulation.

Keywords: Pacific Ocean, Scotia Sea, bottom sediments, Neopleistocene, Eopleistocene

DOI: 10.1134/S0024490220040045

INTRODUCTION

The present paper continues the series of works dedicated to Pleistocene deposits in the World Ocean based on the volumetric method proposed by A.B. Ronov (1949) and the compilation of general lithofacies maps on scales 1 : 35000000, 1 : 20000000, or 1 : 10000000 (Levitan and Gel'vi, 2016; Levitan et al., 2013, 2014, 2018a; and others). Compilation of these maps is based on the deep-sea drilling data and, partly, long sediment cores retrieved during R/V cruises of different countries.

As is known, DSDP sites are located irregularly over the World Ocean. In particular, drilling sites are scarce in several large regions of the Arctic Ocean, South Pacific, and SW Indian Ocean. Moreover, such sites are lacking at all in some seas, e.g., Okhotsk and Scotia.

The present paper is based completely on materials pertaining to lithology and magnetic stratigraphy of long (up to 18 m) sediment cores retrieved by R/V *Eltanin* (United States) during several cruises in the South Ocean in the 1950s–1960s (Goodell and Watkins, 1968).

The aim of our work was to study the facies structures and quantitative parameters of Pleistocene sedimentation on the deep-sea floor of the southern Pacific and in the Scotia Sea.

MATERIALS AND METHODS

Location of long sediment cores retrieved in the southern Pacific and Scotia Sea during cruises of R/V *Eltanin* is shown in Figs. 1 and 2, correspondingly. Data on lithology of the recovered sections and their stratigraphic subdivision based on magnetostratigraphy are given in (Goodell and Watkins, 1968).

We accepted the Pleistocene subdivision based on the old scale (Gradstein et al., 2004): Neopleistocene corresponds, in general, to the Brunhes magnetic chron (except Holocene), i.e., middle and late Pleistocene (roughly from 0.8 to 0.01 Ma). Eopleistocene corresponds to a part of the Matuyama magnetic chron (from the Brunhes boundary to the top of the Olduvai subchron), i.e., early Pleistocene (roughly from 1.8 to 0.8 Ma).

Schematic thickness of the Brunhes and Matuyama sediments is presented by the above-mentioned American researchers for the southern Pacific. For the purposes of our work, thickness of the Matuyama sediments is reduced, taking into consideration duration of the segment extending from the Brunhes/Matuyama boundary to the Olduvai subchron top and assuming uniform sedimentation rate during this time. This process was controlled by the data presented in (Goodell and Watkins, 1968) for the position of the Olduvai subchron top in specified sediment cores.

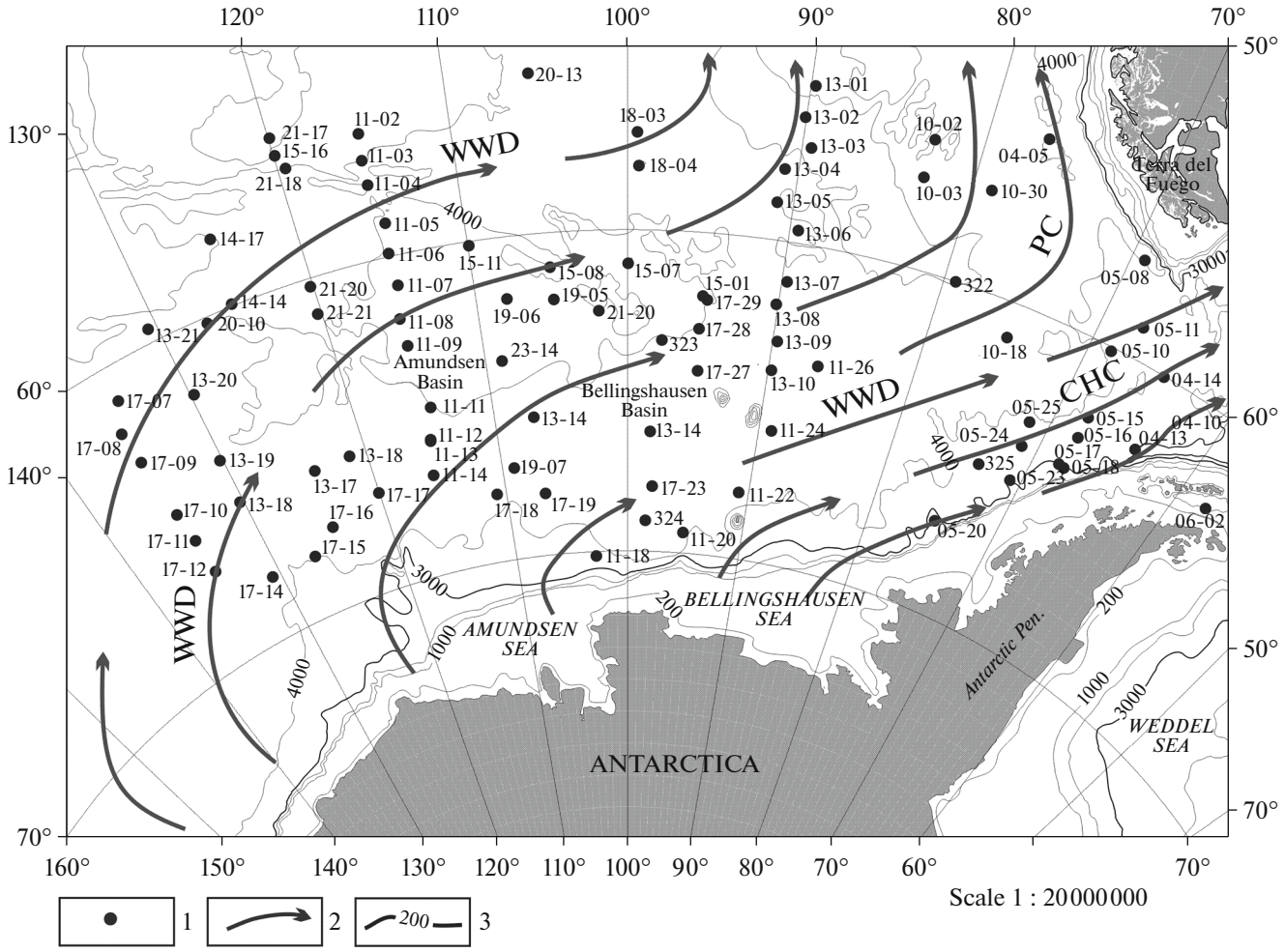

Fig. 1. Location of long sediment cores retrieved by R/V *Eltanin* (United States) (Goodell and Watkins, 1968) and surface currents (Koshlyakov and Tarakanov, 1999) in the southern Pacific. (1) Sediment cores retrieved by R/V *Eltanin*; (2) surface currents; (3) isobaths (m). (WWD) West Wind Drift; (PC) Peru Current; (CHC) Cape Horn Current.

To compile Neo- and Eopleistocene lithofacies maps on scale 1 : 20000000 for the southern Pacific (Figs. 3, 4) and scale 1 : 10000000 for the Scotia Sea (Figs. 5, 6), we used the General Bathymetric Chart of the Oceans (GEBCO) presented in (*General* ..., 2004).

Since thickness chart of sediments is not given for the Scotia Sea in the above-mentioned work, we compiled isopachite charts for the Neopleistocene and Eopleistocene deposits on scale 1 : 10000000, and isopachites were drawn on the respective lithofacies maps (Figs. 5, 6).

In addition to these peculiarities in the location of Pleistocene sections and taking into consideration the absence of information about the Pleistocene sedimentation in DSDP 35 holes (Hollister et al., 1976), we were compelled to combine data on the southern Pacific and Scotia Sea because of an "oceanographic reason": both regions are intersected by the Circum-Antarctic Current, the most powerful current in the World Ocean governing the distribution of diatom oozes and clays on the seafloor in the southern silica deposition belt.

PRESENT-DAY CONDITIONS OF SEDIMENTATION

South Pacific

Seafloor in the area under consideration is limited by the following coordinates: 55° S from the north, 140° W from the west, 60° W from the east, and isobath of 3000 m from the south (Fig. 1). Large morphological elements in the north are represented by a fragment of the South Pacific Rise. Most part of the seafloor is occupied by the Amundsen and Bellingshausen basins. The study area is limited by the submarine continental margin of West Antarctica and the Scotia Sea in the east.

The surface of West Antarctica is covered by the West Antarctic ice sheet. Some glaciologists believe that this region includes an autonomous ice sheet of

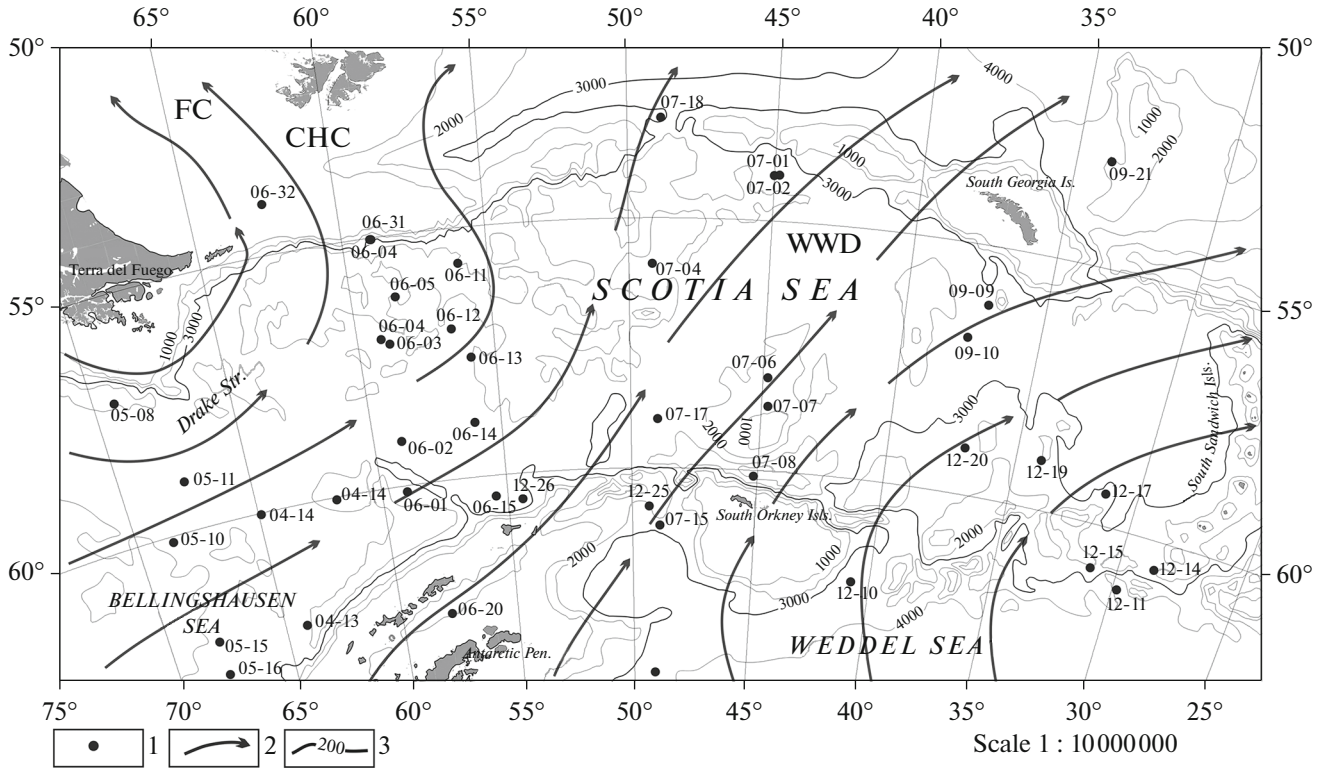

Fig. 2. Location of long sediment cores retrieved by R/V *Eltanin* (United States) (Goodell and Watkins, 1968) and surface currents (Koshlyakov and Tarakanov, 1999) in the Scotia Sea. (1) Sediment cores retrieved by R/V *Eltanin*; (2) surface currents; (3) isobaths (m). (WWD) West Wind Drift; (FC) Falkland Current; (CHC) Cape Horn Current.

the Antarctic Peninsula, and large coastal spaces of this peninsula lack the ice sheet (Ingólfsson, 2004). The northern side of the coastline is covered with sea ice: its northern boundary is located at 65°–70° S in summer and at 55°–58° S in winter (Gersonde et al., 2005).

Water circulation here is dominated by six (mainly sublatitudinal and NE-oriented) streams of the Circum-Antarctic Current (West Wind Drift) that turn to north in the northeastern part of the region (Koshlyakov et al., 2019). Its manifestation at the northeastern edge is represented by the Peru Current. After falling into the Scotia Sea, the West Wind Drift is transformed into the E- and NE-oriented Cape Horn Current (Fig. 1). As is known, water discharge in the Circum-Antarctic Current is as much as 125–160 Sv. The current reaches the seafloor and is several hundred miles wide at 57°–65° S (Hiscock et al., 2003; Koshlyakov and Tarakanov, 1999). Its speed varies from 0.11 to 0.25 m/s in the bottom layer and increases toward the ocean surface (Orsi et al., 1995). During the Pleistocene, fluctuations of its position were at least several dozen miles (Lyle et al., 2007). Water temperature varies from –1.5°C near the ice edge to +4.5°C in summer at the Polar Front located at the northern boundary of the Circum-Antarctic Current. In general, the study area represents an oligotrophic structure, and its annual primary productivity varies from almost zero in winter in the Southern Hemisphere to 80–90 g C/m^2/yr in summer at the Polar Front (Hiscock et al., 2003).

On the whole, the wide zone of submarine margin and abyssal plains is mainly occupied at present by various genetic types of terrigenous deposits that give way northward to an intermittent sublatitudinal zone of diatom oozes and clays and to pelagic carbonate sediments in the north (McCoy et al., 2003).

Let us remind that the southern belt of silica deposition scrutinized in (Lisitsyn, 1966) envelopes the entire Antarctica. This belt comprises diatom sediments with the biogenic opal content reaching 70 wt % in the surface layer (Lisitsyn, 1966) and even as much as 100 wt % in some places (Levitan, 1975). Diatom algae are developed in the surficial water mass of the Circum-Antarctic Current. They are consumed actively by zooplankton organisms (salps, suphausiids, and copepods), and some species of the krill copepods account for as much as 70% of the consumed diatoms (K.N. Kosobokova, 2019, personal communication). The subsidence rate of diatom frustules after its death is negligible, and actually they cannot reach the seafloor independently. However, they descend at a rate of 40–4000 m/d in the composition of fecal pellets of zooplankton that are appreciably larger and heavier

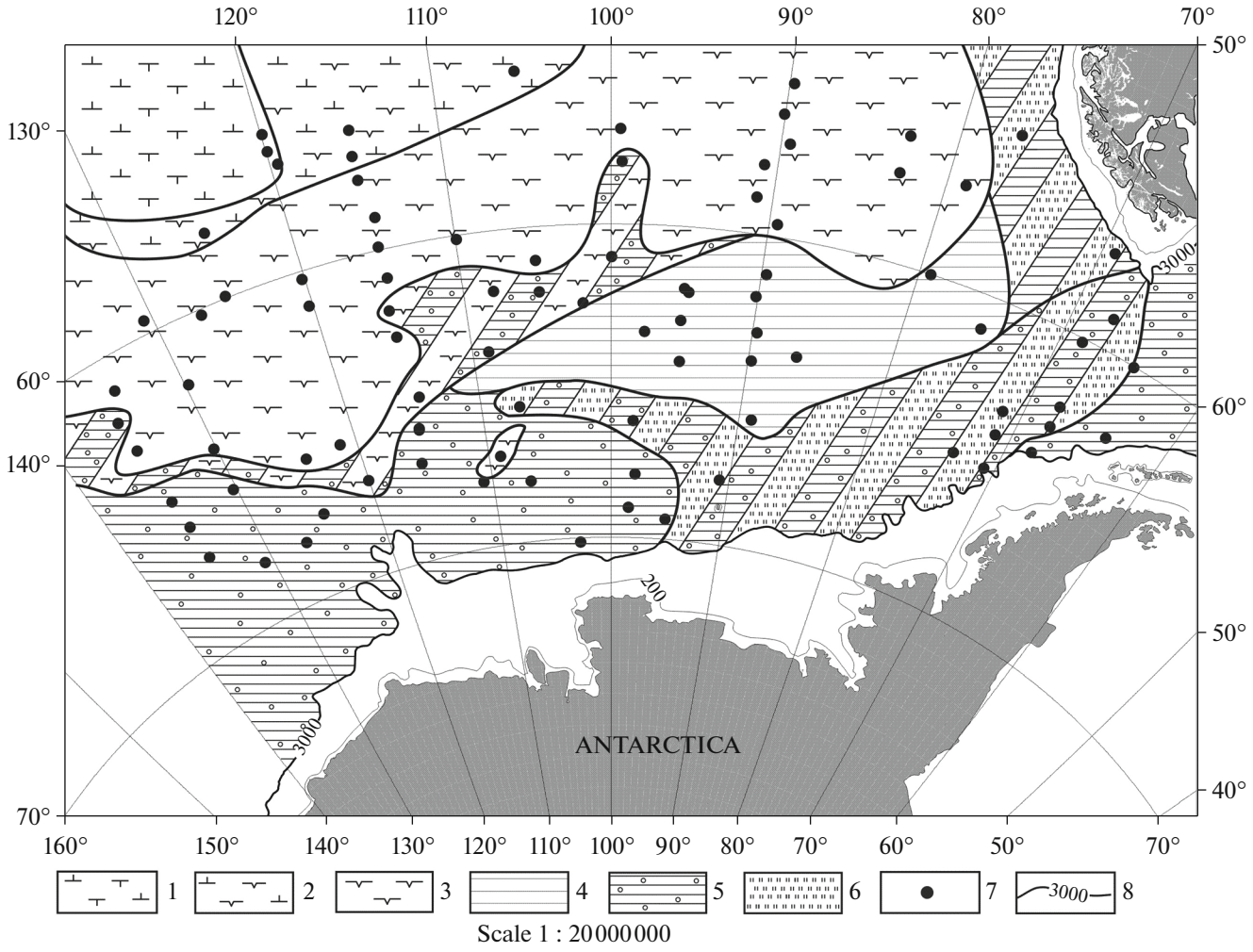

Fig. 3. Lithofacies map of Neopleistocene deposits in the southern Pacific. (1) Coccolith-foraminiferal oozes; (2) coccolith-diatom oozes; (3) diatom oozes and clays; (4) hemipelagic clays; (5) hemipelagic clays with IRD; (6) terrigenous turbidites; (7) sediment cores retrieved by R/V *Eltanin*; (8) isobaths (m).

than individual diatom frustules. Therefore, they can only be accumulated on the seafloor slightly eastward (due to currents) of the primary habitat, because pellets on the seafloor rapidly lose the adhesive organic matter and break down into elementary components, resulting in the release of intact diatom frustules and their detritus (I.N. Sukhanova, 2019, personal communication).

It is noteworthy that an important role in the development of diatoms belongs to the continental input of nutrients during sea ice melting in the course of vertical circulation and ascent of the nutrient-rich deep water to the ocean surface in the Antarctic divergence zone (Polar Front) (Lisitsyn, 1966).

Scotia Sea

The Scotia Sea is adjacent to the submarine North Scotia Ridge in north; to the submarine South Scotia Ridge with the South Orkney Islands in south; and to an island arc crowned by the South Sandwich Islands in east (Udintsev and Shenke, 2004). In north, the South Scotia Ridge is adjacent to a sublatitudinal rift of the Bransfield Strait more than 4000 m deep. From the geodynamic point of view, the Scotia Sea is an island-arc margin of the Atlantic Ocean and represents a back-arc basin.

Area of the sea is about 1.3 mln km^2, average depth is slightly more than 3000 m, and maximum depth is 6022 m (Pospelov, 2002). We can assume conventionally that the Scotia Sea comprises two major (western and eastern) parts. Seafloor in the western part is composed of the spreading-type oceanic crust. The corresponding median ridge is crosscut by several large NW-striking transform faults. On the whole, the northern half of the study region is characterized by a greater depth (as much as 5000 m). The eastern part, mainly composed of seamounts and microcontinent

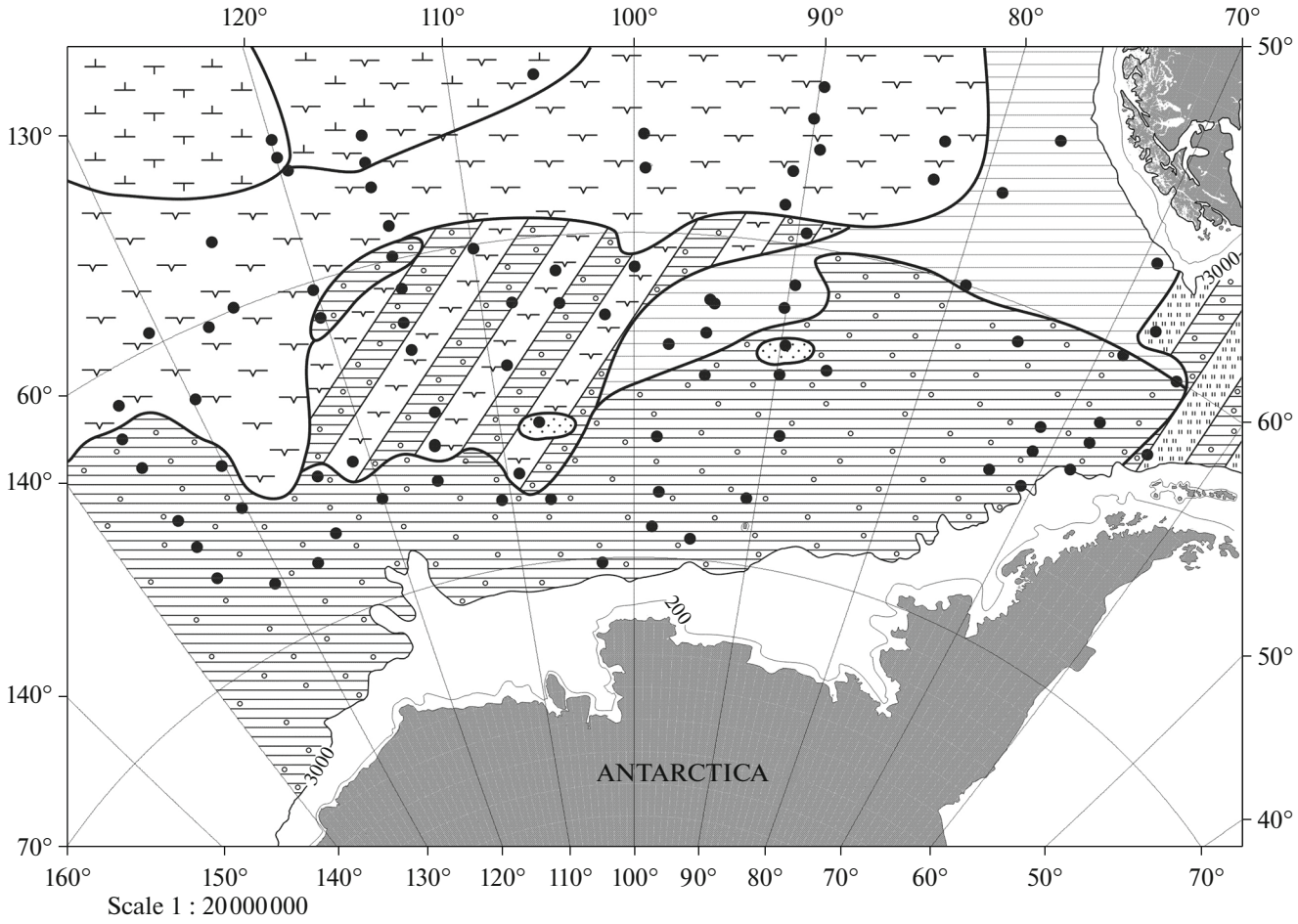

Fig. 4. Lithofacies map of Eopleistocene deposits in the southern Pacific. Legend as in Fig. 3.

banks, is characterized by depths ranging from 1500 to 3500 m (*General ...*, 2004).

Average water temperature on the surface varies from 6°C to –1°C, and salinity is approximately 34‰. Temperate latitude waters are only confined to the northwestern part of the Scotia Sea. The middle part is dominated by the southern polar water of the Circum-Antarctic Current. From the south, an even colder water of the Weddell Sea flows to the southeastern part. The Weddell Sea is a major area of the Antarctic iceberg origin. Primary productivity in the coastal water near the South Orkney and South Sandwich islands varies from 13 to 45 mg C/m^2/d; in the central part of the sea, from 1.8 to 3.0 mg C/m^2/d (Volkovinskii, 1969).

At present, a large seafloor area in the eastern and central parts of the basin is covered by diatom oozes and clays (Emel'yanov et al., 1975). Low-carbonate and carbonate planktonic oozes are developed on the South Scotia Ridge and northern side of the western Weddell Sea. A similar ooze zone is developed in the southwestern part of the region.

RESULTS

South Pacific

Neopleistocene. The Neopleistocene period was marked generally by a lithofacies zonation (Fig. 3) similar to the present-day pattern. It demonstrates the following general zonation: in the northwest, a small foraminiferal-coccolith ooze zone is confined to the South Pacific Rise with relatively small depths; on the eastern side, this zone gives way to a diatom-coccolith ooze zone, because this area is already affected by the West Wind Drift (Circum-Antarctic Current); and almost one-half of the northern part is occupied by siliceous sediments together with diatom oozes and clays that are not shown separately in (Goodell and Watkins, 1968). These deposits outline rather discretely the Circum-Antarctic Current terrain. Finally, a large terrain of terrigenous deposits is located on the southern and eastern sides via a narrow zone of intercalating siliceous sediments and hemipelagic clays. Unfortunately, the description of structures and textures of these deposits is lacking in the above-cited work. Therefore, we assumed that the wide distribution of sand in Neopleistocene deposits is related to

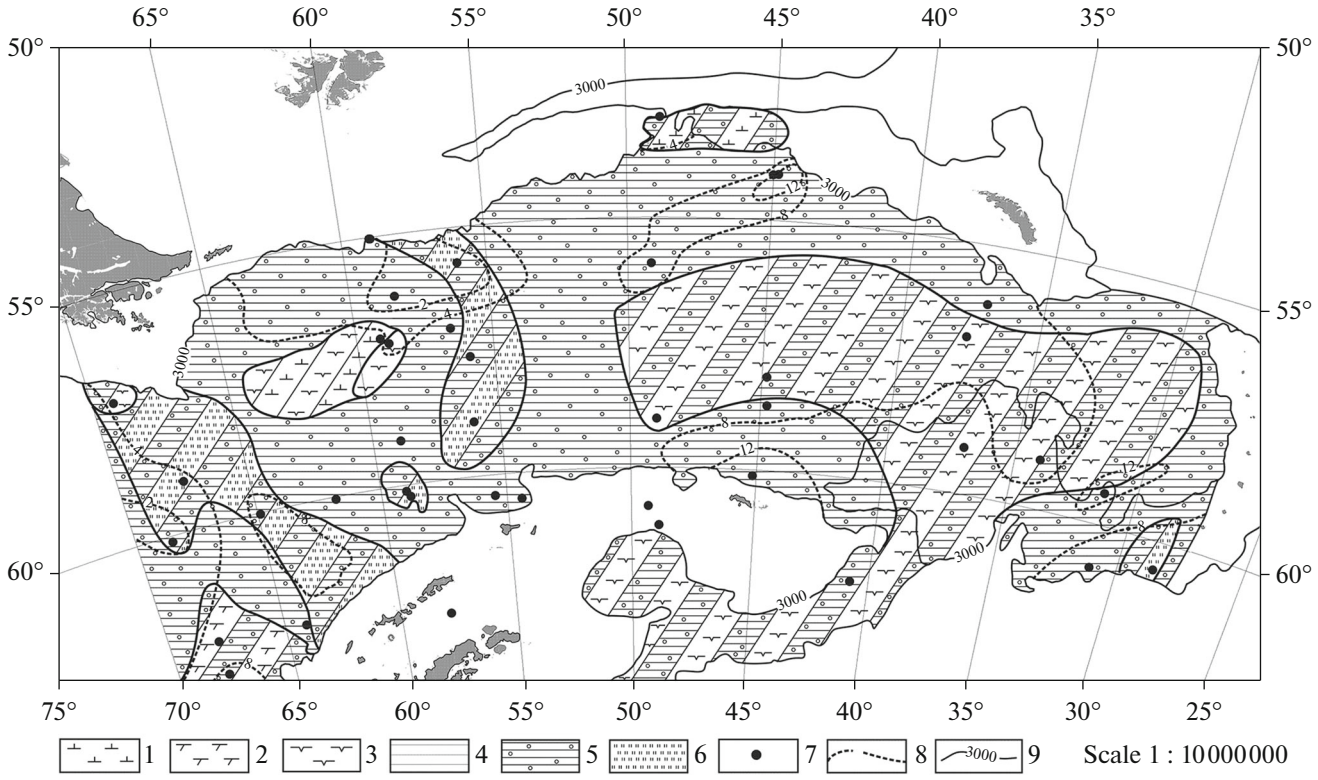

Fig. 5. Lithofacies map of Neopleistocene deposits in the Scotia Sea. (1) Coccolith oozes; (2) foraminiferal oozes; (3) diatom oozes and clays; (4) hemipelagic clays; (5) hemipelagic clays with IRD; (6) terrigenous turbidites; (7) sediment cores retrieved by R/V *Eltanin*; (8) isopachites (m); (9) isobaths (m).

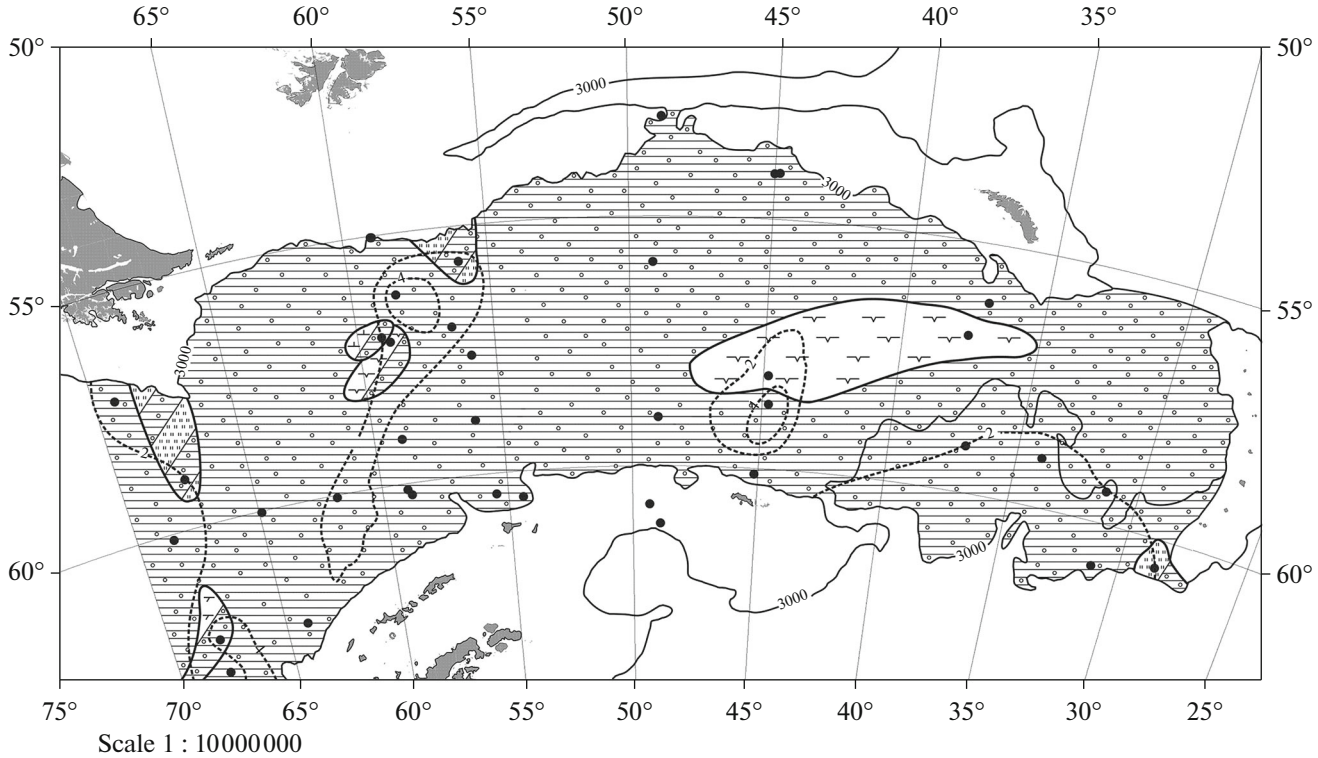

Fig. 6. Lithofacies map of Eopleistocene deposits in the Scotia Sea. Legend as in Fig. 5.

Table 1. Areas (S, thou km^2) and volumes (V, thou km^3) of Pleistocene deposits in the southern Pacific

Lithology	Foraminiferal-coccolith oozes		Coccolith-diatom oozes and clays		Diatom oozes and clays		Terrigenous turbidites		Hemipelagic clays with IRD		Hemipelagic clays	
Neopleistocene	*S*	*V*	*S*	*V*	*S*	*V*	*S*	*V*	*S*	*V*	*S*	*V*
	449.0	0.7	521.7	4.6	3107.8	19.9	1254.2	6.4	1404.2	4.7	463.9	0.84
Eopleistocene	358.7	0.21	329.0	0.53	3044.2	6.37	81.1	6.0	3921.2	13.1	342.3	0.52

Table 2. Masses of dry sediment (M, 10^{18} g) and sediment per unit time (I, 10^{18} g/Ma) in the southern Pacific

Age	Foraminiferal-coccolith oozes		Coccolith-diatom oozes and clays		Diatom oozes and clays		Hemipelagic clays c IRD		Hemipelagic clays		Terrigenous turbidites		Sands	
	M	*I*	*M*	*I*	*M*	*I*	*M*	*I*	*M*	*I*	*M*	*I*	*M*	*I*
Neopleistocene	0.525	0.66	2.76	3.49	8.358	10.58	20.224	25.6	0.586	0.74	4.608	5.83	0	0
Eopleistocene	0.158	0.16	0.398	0.4	4.449	4.45	7.119	7.12	0.379	0.38	0.792	0.79	0.127	0.13

the presence of proximal turbidites intercalating with the hemipelagic clays *sensu lato* (i.e., deposits including not only the pelitic sediments but also the aleuritic-pelitic and fine-aleuritic varieties and coarse aleurites). Correspondingly, we can define two terrigenous sediment terrains: (1) hemipelagic clays (with or without the ice-rafted detritus, IRD); (2) intercalation of similar hemipelagic clays and terrigenous turbidites confined to southeast and east of the given region.

Thickness of Neopleistocene deposits is minimal (0–2 m) in the carbonate ooze terrain, increases to 12 m in the northernmost part, varies from 2 to 8 m in the central part, and again increases to 12 and even 16 m in the southern and northeastern parts (nearer to the terrigenous sedimentary provenance, i.e., Antarctica and South America) (Goodell and Watkins, 1968).

The results of examination of the above-mentioned map based on consideration of the thickness data and the volumetric method (Ronov, 1949) are presented in Tables 1 and 2. When recalculating the volume of sediments (Table 1) into the dry sediment mass (Table 2), we took into account the data on physical properties of deposits reported in (Levitan et al., 2014, 2018b).

Neopleistocene deposits are developed over 7092 thou km^2 and their total volume is 63.6 km^3 (Table 1). Their terrain can be divided into the following zones: diatom oozes and clays (2606.7 thou km^2); hemipelagic clays with IRD (1646.1 thou km^2); terrigenous turbidites intercalating with hemipelagic clays and including IRD (903.1 thou km^2); coccolith-diatom oozes and clays (521.7 thou km^2); diatom oozes and clays intercalating with hemipelagic clays and including IRD (501.1 thou km^2); foraminiferal-coccolith oozes (449.0 thou km^2); intercalating terrigenous turbidites and hemipelagic clays (351.1 thou km^2); and hemipelagic clays (112.8 thou km^2).

In terms of percentage from the total volume, distribution of Neopleistocene deposits makes up the following series: (1) hemipelagic clays with IRD (48.92%); diatom oozes and clays (31.24%); (2) terrigenous turbidites (10.05%); (3) coccolith-diatom oozes and clays (7.22%); (4) hemipelagic clays without IRD (1.32%); and (5) foraminiferal-coccolith oozes (1.10%).

Distribution of the dry sediment mass makes up the following series (in 10^{18} g): (1) hemipelagic clays with IRD (20.224); (2) diatom oozes and clays (8.358); (3) terrigenous turbidites (4.608); (4) coccolith-diatom oozes and clays (2.760); and (5) hemipelagic clays without IRD and foraminiferal-coccolith oozes (approximately 0.5–0.6 each) (Table 2).

Variation in the dry sediment mass per unit time is as follows (in 10^{18} g/Ma): (1) hemipelagic clays with IRD (25.6); (2) foraminiferal-coccolith oozes (0.53) (Table 2).

Eopleistocene. Facies distribution in the Eopleistocene (Fig. 4) was basically similar to the Neopleistocene pattern, but the terrain of intercalating terrigenous turbidites and hemipelagic clays was notably smaller and only existed in the southeastern part of the region under consideration.

It should be noted that Eopleistocene deposits are significantly thinner than the Neopleistocene variety (Goodell and Watkins, 1968). One should take into mind, however, that the complete section of Eopleistocene deposits has been recovered by a much lesser number of DSDP wells, relative to the Neopleistocene section. Nevertheless, the thinning of all main lithological (carbonate, siliceous, and terrigenous) deposits is evident. For example, thickness of Eopleistocene deposits is not more than 1 m at some places in northwest, varies from 2 to 8 m in the central zone, slightly more than 6 m in south, and approximately 2–4 m in northeast (Fig. 4).

The Eopleistocene deposits are developed over 7090.4 thou km^2 and their total volume is 22.69 km^3 (Table 1). In terms of area, Eopleistocene terrains are arranged in the following way: (1) hemipelagic clays with IRD (2906.3 thou km^2); (2) diatom oozes and clays (2110.4 thou km^2); (3) intercalation of diatom oozes and clays with hemipelagic clays including IRD (933.8 thou km^2); (4) foraminiferal-coccolith oozes (358.7 thou km^2); (5) hemipelagic clays (342.3 thou km^2); (6) coccolith-diatom oozes and clays (329.0 thou km^2); (7) intercalation of terrigenous turbidites with hemipelagic clays including IRD (81.1 thou km^2); and (8) sands (28.8 thou km^2).

In terms of percentage from the total volume, Eopleistocene terrains are arranged in the following way: (1) hemipelagic clays with IRD (59.80%); (2) diatom oozes and clays (28.05%); (3) terrigenous turbidites (4.85%); (4) coccolith-diatom oozes and clays (2.34%); (5) hemipelagic clays without IRD (2.29%); (6) foraminiferal-coccolith oozes (0.93%); and (7) sands 0.14%.

Variation in the dry sediment mass makes up the following series (in 10^{18} g): (1) hemipelagic clays with IRD (7.119); (2) diatom oozes and clays (4.449); (3) terrigenous turbidites (0.792); (4) coccolith-diatom oozes and clays (0.398); (5) hemipelagic clays without IRD (0.379); (6) foraminiferal-coccolith oozes (0.158); and (7) sands (0.127) (Table 2).

A similar series is recorded for variation in the dry sediment mass per unit time in the Eopleistocene (in 10^{18} g/Ma): (1) hemipelagic clays with IRD (7.119); (2) sands (0.127) (Table 2).

Based on the Neopleistocene/Eopleistocene ratio of the distribution of dry sediment mass per unit time, we get the following series: (1) hemipelagic clays with IRD (3.60); (2) diatom oozes and clays (2.38); (3) terrigenous turbidites (7.38); (4) coccolith-diatom oozes and clays (8.73); (5) hemipelagic clays without IRD (1.95); (6) foraminiferal-coccolith oozes (4.13); and (7) sands (0).

Scotia Sea

Neopleistocene. In the Neopleistocene, seafloor in the western part of the region under consideration was marked by the accumulation of mainly hemipelagic clays with IRD (Fig. 5). Between 53° and 64°W, their terrain gave way to a submeridional zone of the intercalation of similar clays with proximal terrigenous turbidites. Another zone with such sediments extends along the northwestern direction from 60° to 70°W. A subordinate terrain of the intercalation of diatom oozes and clays with coccolith oozes is located at the center of the western part on the northern slope of the spreading ridge. Finally, the shallow-water area at the southwestern corner of the region accommodates a small patch of the intercalation of hemipelagic clays with IRD and foraminiferal oozes.

In the eastern part of the basin, the main area of the seafloor is occupied by intercalations of diatom oozes and clays with hemipelagic clays containing the IRD. This terrain is surrounded by the monofacies hemipelagic clays with IRD. A small spot of the intercalation of coccolith oozes and hemipelagic clays with IRD is only recorded on the North Scotia Ridge, and the intercalation of terrigenous turbidites and hemipelagic clays with IRD is observed at the southeastern edge of the basin.

Neopleistocene deposits are thickest (from 8 to 12 m or more) near the sources of terrigenous material provinces along the basin periphery, and they are thinnest in the central part of the Scotia Sea (Fig. 5).

Neopleistocene deposits are developed over 1833.7 thou km^2 and their total volume is 13.0 km^3 (Table 3). In terms of area, their terrains make up the following series: (1) hemipelagic clays with IRD (927.3 thou km^2; (2) intercalation of diatom oozes and clays with hemipelagic clays including IRD (571.0 thou km^2); (3) intercalation of terrigenous turbidites and hemipelagic clays with IRD (213.4 thou km^2); (4) intercalation of foraminiferal oozes and hemipelagic clays with IRD (38.8 thou km^2); (5) intercalation of sediments and diatom oozes with coccolith oozes (37.3 thou km^2); (6) intercalation of coccolith oozes and hemipelagic clays with IRD (29.5 thou km^2); (7) diatom oozes and clays (8.6 thou km^2); and (8) their intercalation with terrigenous turbidites (7.6 thou km^2).

In terms of percentage from the total volume (Table 3), Neopleistocene deposits make up the following series: (1) hemipelagic clays with IRD (87.1%); (2) diatom oozes and clays (6.8%); (3) terrigenous turbidites (4.2%); (4) foraminiferal oozes (1.5%); and (5) coccolith oozes (0.4%).

In terms of the dry sediment mass, the series is as follows (in 10^{18} g): (1) hemipelagic clays with IRD (7.238); (2) terrigenous turbidites (0.389); (3) diatom oozes and clays (0.372); (4) foraminiferal oozes (0.176); and (5) coccolith oozes (0.038) (Table 4).

Variation of the dry sediment mass per unit time in the Neopleistocene demonstrate a similar series (in 10^{18} g/Ma): (1) hemipelagic clays with IRD (9.16); (2) coccolith oozes (0.05) (Table 4).

Eopleistocene. In the Eopleistocene, the Scotia Sea floor was occupied almost completely by the hemipelagic clays with IRD (Fig. 6). The southeastern margin and northwestern part of the basin included small patches of the intercalation of such clays with terrigenous turbidites. Analogous clays intercalated with coccolith or diatom oozes and clays at the center in the western half of the sea, but with foraminiferal clays in the southwest. Finally, a sufficiently large area at the

Table 3. Areas (S, thou km^2) and volumes (V, thou km^3) of Pleistocene deposits in the Scotia Sea

Age	Hemipelagic clays with IRD		Diatom oozes and clays		Terrigenous turbidites		Foraminiferal clays		Coccolith oozes		∑S (total mass of sediments)	∑V (total volume of sediments)
	S	*V*	*S*	*V*	*S*	*V*	*S*	*V*	*S*	*V*		
Neopleistocene	1780	11.31	624.7	0.886	221.2	0.54	38.8	0.2	66.8	0.05	1833.7	13.0
Eopleistocene	1728.6	2.48	114.9	0.104	28.7	0.03	11.8	0.03	6.0	0.001	1831.4	2.65

Table 4. Masses of dry sediment (M, 10^{18} g) and sediment per unit time (I, 10^{18} g/Ma) of Pleistocene deposits in the Scotia Sea

Age	Hemipelagic clays with IRD		Diatom oozes and clays		Terrigenous turbidites		Foraminiferal oozes		Coccolith oozes	
	M	*I*	*M*	*I*	*M*	*I*	*M*	*I*	*M*	*I*
Neopleistocene	7.238	9.16	0.372	0.47	0.389	0.49	0.176	0.22	0.038	0.05
Eopleistocene	1.587	1.587	0.044	0.044	0.022	0.022	0.026	0.026	0.001	0.001

center in the eastern half of the Scotia Sea floor was occupied by diatom oozes and clays.

Thickness of Eopleistocene deposits is obviously lesser relative to the Neopleistocene bottom deposits: almost the whole area was covered with thin (<2 m) deposits. The deposits are thicker (slightly more than 4 m) only at the basin center, as well as in the southwestern and northern sectors of the western part (Fig. 6).

Eopleistocene deposits are developed over 1831.4 thou km^2 and their total volume is 2.65 km^3 (Table 3). In terms of area, their terrains make up the following series: (1) hemipelagic clays with IRD (1670.0 thou km^2), (2) diatom oozes and clays (102.8 thou km^2); (3) intercalation of terrigenous turbidites and hemipelagic clays with IRD (28.7 thou km^2); (4) intercalation of diatom oozes and clays with hemipelagic clays including IRD (12.1 thou km^2); (5) intercalation of foraminiferal oozes and hemipelagic clays with IRD (11.8 thou km^2); and (6) intercalation of coccolith oozes and hemipelagic clays with IRD (6.0 thou km^2).

In terms of percentage from the total volume (Table 3), Eopleistocene deposits make up following series: (1) hemipelagic clays with IRD (93.8%); (2) diatom oozes and clays (3.9%); (3) terrigenous turbidites (1.1%); (4) foraminiferal oozes (1.1%); and (5) coccolith oozes (0.04%).

In terms of distribution of the dry sediment mass, the series is as follows (in 10^{18} g): (1) hemipelagic clays with IRD (1.587); (2) diatom oozes and clays (0.044); (3) foraminiferal oozes (0.026); (4) terrigenous turbidites (0.022); and (5) coccolith oozes (0.001) (Table 4).

In terms of variation in the dry sediment mass per unit time in the Eopleistocene, the series is as follows (in 10^{18} g/Ma): (1) hemipelagic clays with IRD (1.59); (2) coccolith oozes (0.001) (Table 4).

Based on the Neopleistocene/Eopleistocene ratio of distribution of the dry sediment mass per unit time, we get the following series: (1) hemipelagic clays with IRD (5.77); (2) diatom oozes and clays (10.68); (3) terrigenous turbidites (22.27); (4) foraminiferal oozes (8.46); and (5) coccolith oozes (50.00).

DISCUSSION

South Pacific

This region is dominated by terrigenous deposits. Relative to the Eopleistocene, the Neopleistocene was characterized by 3.82 times higher rate of the accumulation of terrigenous sediments and 7.38 higher rate of the accumulation of terrigenous turbidites.

In terms of accumulation rate, the second place belongs to the group of siliceous (diatom-rich) sediments: their accumulation rate in the Neopleistocene was 2.65 times higher than in the Eopleistocene.

Finally, the group of planktogenic carbonate sediments, which occupies the least volume among Pleistocene deposits, was accumulated 6.82 times rapidly in the Neopleistocene than in the Eopleistocene.

Thus, all main sediment groups are characterized by a higher sedimentation rate in the Neopleistocene relative to the Eopleistocene. Similar trends are also typical of the entire Pacific Ocean over its pelagic zone and submarine continental margins (Levitan, 2020).

We believe that such trend in the southern Pacific is related, first of all, to neotectonic activity in the Alpine Andian foldbelt extending (with local hiatuses) further southward to the Scotia island-arc, Antarctic Peninsula, and continental margin of the Pacific segment of the South Sea. Moreover, the Pleistocene period was characterized by a higher influx of not only terrigenous material, but also nutrients transported by melted waters from the West Antarctic ice sheet.

Scotia Sea

This region also demonstrates trends similar to those in the southern Pacific: predominance of terrigenous sedimentation, presence of diatom oozes, and suppressed role of the planktogenic carbonate sedimentation. Here, the accumulation rate of all sediment groups in the Neopleistocene was higher than in the Eopleistocene (6.00 times higher for the terrigenous group, 8.46 times higher for the siliceous group, and 10.04 times higher for the carbonate group). Correspondingly, reasons for these regularities are the same as those noted above.

Spatiotemporal Variability of Pleistocene Accumulation within the Southern Belt of Silica Deposition

The results reported in this paper coupled with our previous data on the Indian (Levitan et al., 2014) and Atlantic (Levitan and Gel'vi, 2016) oceans provide insight into variations in the diatom accumulation rate during the Pleistocene within the southern belt of silica deposition.

Our data on the Pleistocene can be described in the following concise form: the rate of biogenic opal accumulation was decreased during Pleistocene in the Indian segment of the southern belt of silica deposition and increased in the Pacific Ocean and Scotia Sea. However, intensity of the accumulation of diatom sediments in the Weddell Sea (southern Atlantic Ocean) was retained at approximately the same rate as in the Pleistocene (from 1.8 to 0.01 Ma ago).

To explain the above-described peculiarities of silica deposition, it will be expedient to analyze the glacial and paleoglacial data on the Antarctic ice sheets with due consideration of modern concepts of the geological structure of Antarctica.

Let us remind that the East Antarctic Shield is located in harshest climatic conditions, with the basement composed of ancient Antarctic Platform bedrocks and Early Paleozoic reactivation belts (Khain, 2001). Our previous data on the mobility of this shield suggest its extremely low mobility: the prevalent delivery of terrigenous material to basins of the South Sea was related mainly to "bulldozer-type" advances of the ice sheet margin to shelf boundaries during glaciations (Levitan and Leichenkov, 2014), whereas nutrients were delivered with melted waters mainly during interglacials. Let us remind that the Eopleistocene period, in general, was appreciably warmer than the Neopleistocene (Lisiecki and Raymo, 2005). Information about active neotectonic movements in East Antarctica is virtually absent.

In contrast, the polythermal ice sheet in West Antarctica (particularly, in the Antarctic Peninsula), is situated in more favorable climatic conditions (Ingólfsson, 2004). Its margins are resting on seawater. During the middle Miocene (approximately 14 Ma ago), this sheet occupied the Cenozoic rift zone of West Antarctica and island archipelago crowning an island arc in the west. Therefore, this sheet was much more mobile than the eastern neighbor. For example, during the Pliocene thermal maximum, the volume of melted water corresponded to 20-m rise of the World Ocean level, while the volume of melted water in the East Antarctic Shield was just 5 m (Naish, 2010). Correspondingly, glacial–interglacial cycles in the West Antarctic Shield promoted the delivery of a huge amount of both suspended sedimentary material and dissolved nutrients together with the melted waters. This process was accompanied by the neotectonic orogenic movements that took place more vigorously in the Neopleistocene than in the Eopleistocene, as suggested by the data on terrigenous turbidites presented above.

The Weddell Sea is marked by the combination of fluxes of nutrients (phosphates, nitrates, and some metals, such as Fe in the bioavailable form) in meltwaters from both ice sheets. Therefore, intensity of silica deposition in the Eopleistocene and Neopleistocene was approximately equal (Levitan and Gel'vi, 2016).

Thus, differences in the tectonics (and neotectonics) and paleoglaciology of West and East Antarctica were responsible for the above-described spatiotemporal discrepancies in the diatom ooze deposition in the Pleistocene within the southern belt of silica deposition, because precisely the delivery of nutrients ultimately governs this process via the vertical water circulation.

CONCLUSION

Based on the data pertaining to long bottom sediment cores retrieved during the cruise of R/V *Eltanin*, United States (Goodell and Watkins, 1968), we compiled the lithofacies maps for all age sections of the Neopleistocene and Eopleistocene in the southern Pacific and Scotia Sea. The map scale was 1 : 20000000 for the southern Pacific and 1 : 10000000 for the Scotia Sea. Distribution of the thickness of respective deposits in the southern Pacific was adopted from the above-cited work. For the Scotia Sea, we compiled the maps based on our data and drew isopachites on the lithofacies maps.

Using the volumetric method proposed by A.B. Ronov, we computed quantitative parameters of sedimentation for all maps. The results revealed that both regions are characterized by the intensification of not only terrigenous but also siliceous sedimentation in the Neopleistocene, relative to the Eopleistocene. The carbonate accumulation was subordinate. The regularities described above are likely related mainly to the delivery of nutrients from tectonically active zones of the West Antarctica due to specific dynamics of the West Antarctic ice sheet in the Pleistocene. These data made it possible to refine significantly the map of spa-

tial variation in the southern silica deposition belt in the Pleistocene.

The presented new maps of the southern Pacific and quantitative parameters of sedimentation computed for the Neopleistocene and Eopleistocene periods suggest that corresponding corrections should be made in the previous materials pertaining to the Pleistocene pelagic sediments in the Pacific (Levitan et al., 2013).

FUNDING

This work was accomplished under the Russian State Task (project no. 01372019-0007) and supported by the Russian Academy of Sciences (program no. 20).

REFERENCES

Emel'yanov, E.M., Lisitsyn, A.P., and Il'in, A.V., *Tipy Donnykh osadkov Atlanticheskogo okeana* (Types of Bottom Sediments in the Atlantic Ocean), Kaliningrad: Pravda, 1975, vol. 579.

General Bathymetric Chart of the Oceans (GEBCO), 2004.

Gersonde, R., Crosta, X., Abelmann, A., and Armand, L., Sea-surface temperature and sea ice distribution of the Southern Ocean at the EPILOG Last Glacial Maximum - a circum-Antarctic view based on siliceous microfossil records, *Quat. Sci. Rev.*, 2005, vol. 24, pp. 869–896.

Goodell, H.G. and Watkins, N.D., The paleomagnetic stratigraphy of the Southern Ocean: 20° west to 160° east, *Deep-Sea Res. Oceanogr. Abstracts*, 1968, vol. 15, no. 1, pp. 89–112.

Gradstein, F.M., Ogg, J.G., Smith, A.G., et al., *A Geologic Time Scale 2004*, Cambridge: Cambridge Univ. Press, 2004.

Hiscock, M.R., Marra, J., Smith, Jr.W.O., et al., Primary productivity and its regulation in the pacific sector of the Southern Ocean, *Deep-Sea Res. II*, 2003, vol. 50, pp. 533–538.

Hollister, Ch.D., Craddock, C., Tucholke, B.E., et al., *Init. Repts. DSDP*, 1976, vol. 35.

Ingólfsson Ó., Quaternary glacial and climate history of Antarctica, in *Quaternary Glaciations—Extent and Chronology*, Ehlers, J. and Gibbard, P.L., Eds., Amsterdam: Elsevier, 2004, part 3, pp. 3–43.

Khain, V.E., *Tektonika kontinentov i okeanov (god 2000)* (Tectonics of Continents and Oceans—Year 2000), Moscow: Nauchn. Mir, 2001.

Koshlyakov, M.N. and Tarakanov, R.Yu., Water masses of the Pacific Antarctic, *Oceanology*, 1999, vol. 39, no. 1, pp. 1–11.

Koshlyakov, M.N., Tarakanov, R.Yu., and Savchenko, D.S., Energetic interactions of swirls and whirls in the Antarctic Circumpolar Current in surface layer of the Southern Ocean, *Okeanolog. Issled.*, 2019, vol. 47, no. 3, pp. 39–57.

Levitan, M.A., Biogenic silica as source of material for the formation of cherts in sediments of the Pacific Ocean, *Extended Abstract of PhD (Geol.-Miner.) Dissertation*, Moscow: MGU, 1975.

Levitan, M.A., Balukhovskii, A.N., Antonova, T.A., and Gel'vi, T.N., Quantitative parameters of Pleistocene pelagic sedimentation in the Pacific Ocean, *Geochem. Int.*, 2013, no. 5, pp. 345–352.

Levitan, M.A., Antonova, T.A., and Gel'vi, T.N., Facies structure and quantitative parameters of Pleistocene pelagic sedimentation in the Indian Ocean, *Geochem. Int.*, 2014, no. 4, pp. 316–324.

Levitan, M.A. and Leichenkov, G.L., Cenozoic glaciation of Antarctica and sedimentation in the Southern Ocean, *Lithol. Miner. Resour.*, 2014, no. 2, pp. 117–137.

Levitan, M.A. and Gel'vi, T.N., Quantitative parameters of Pleistocene pelagic sedimentation in the Atlantic Ocean, *Geochem. Int.*, 2016, no. 12, pp. 1049–1060.

Levitan, M.A., Gel'vi, T.N., Syromyatnikov, K.V., and Chekan, K.M., Facies structure and quantitative parameters of Pleistocene sediments of the Bering Sea, *Geochem. Int.*, 2018a, no. 4, pp. 304–317.

Levitan, M.A., Gel'vi, T.N., and Domaratskaya, L.G., Facies structure and quantitative parameters of Pleistocene sediments at the submarine continental margin of Wilkes Land and Ross Sea (Antarctica), *Vestn. IG Komi NTs URO RAN*, 2018b, no. 10, pp. 17–22.

Levitan, M.A., Comparative analysis of Pleistocene sediments of pelagic area and submarine continental margins of the Pacific Ocean, *Geochem. Int.*, 2020, vol. 58, no. 1, pp. 49–60.

Lisiecki, L.E. and Raymo, M.E., A Pliocene-Pleistocene stack of 57 globally distributed benthic $\delta^{18}O$ records, *Paleoceanography*, 2005, vol. 20, PA1003. https://doi.org/10.1029/2004PA001071

Lisitsyn, A.P., Main regularities in the distribution of recent siliceous sediments and their relation to climatic zonation, in *Geokhimiya kremnezema* (Geochemistry of Silica), Moscow: Nauka, 1966, pp. 90–191.

Lyle, M., Gibbs, S., Moore, T.C., and Rea, D.K., Late Oligocene initiation of the Antarctic Circumpolar Current: Evidence from the South Pacific, *Geology*, 2007, vol. 35, no. 8, pp. 691–694.

McCoy, F.W., Swint, T.R., and Piper, D.Z., Types of Bottom sediments, in *Mezhdunarodnyi geologo-geofizicheskii atlas Tikhogo okeana* (International Geological–Geophysical Atlas of the Pacific Ocean), Udintsev, G.B., Ed., Moscow: St. Petersburg, 2003, pp. 114–115.

Naish, T.R., The variability of Pliocene Antarctic ice sheets and implications for global sea-level, *Abstr. IPY Oslo Sci. Conf.*, Oslo, 2010, LM9.2-1.4.

Orsi, A.H., Whitworth, T., and Nowlin, W.D., Jr., On the meridional extent and fronts of the Antarctic Circumpolar Current, *Deep-Sea Res. I*, 1995, vol. 42, no. 5, pp. 641–673.

Pospelov, E.M., *Geograficheskie nazvaniya Mira. Toponimicheskii slovar* (Geographic Names of the World: Toponymic Dictionary), Moscow: Russk. Slovari, 2002.

Ronov, A.B., History of sedimentation and oscillatory movements in the European part of the Soviet Union: Evidence from the volumetric method data, *Tr. Geofiz. Inst. AN SSSR*, 1949, no. 3, p. 136.

Udintsev, G.B. and Shenke, G.V., *Ocherki geodinamiki Zapadnoi Antarktiki* (Essays on the Geodynamics of Western Antarctica), Moscow: GEOS, 2004.

Volkovinskii, V.V., Determinations of primary productivity in the Scotia Sea, *Okeanologiya*, 1969, vol. 66, pp. 160–167.

Translated by D. Sakya